CARBON 79 (2014) 113–122

Available at www.sciencedirect.com

ScienceDirect

journal homepage: www.elsevier.com/locate/carbon

Structural annealing of carbon coated aligned multi-walled carbon nanotube sheets

Shaghayegh Faraji [a], Kelly Stano [a], Christina Rost [b], Jon-Paul Maria [b], Yuntian Zhu [b], Philip D. Bradford [a,*]

[a] Department of Textile Engineering, Chemistry and Science, North Carolina State University, Campus Box 8301, Raleigh, NC 27695, USA
[b] Department of Materials Science and Engineering, North Carolina State University, Campus Box 7907, Raleigh, NC 27695, USA

ARTICLE INFO

Article history:
Received 19 April 2014
Accepted 16 July 2014
Available online 24 July 2014

ABSTRACT

Sheets of aligned multi-walled carbon nanotubes (AMWCNTs) were used to study the structural annealing of pyrolytic carbon (PyC) coatings with various thicknesses on MWCNTs. PyC was deposited using chemical vapor infiltration and the thickness was controlled via the infiltration time. Structural annealing of the PyC coated AMWCNT (AMWCNT/C) sheets at 2150 °C provided different results for different thickness coatings. Transmission electron microscopy images showed that the carbon deposited from acetylene formed laminar PyC coatings, resembling rough tube walls, on the CNT surfaces. Following the high temperature heat treatment, coatings from short PyC deposition times changed their structure, resulting in radial growth of the MWCNTs. Raman and X-ray diffraction measurements also revealed that the radially grown MWCNTs had graphitic quality very close to pristine nanotubes after annealing. Electrical conductivity of AMWCNT/C sheets after high temperature heat treatment was twice that of pristine AMWCNT sheets. The focus of this study was to determine the PyC coating thickness at which a rough PyC coating would no longer change its structure into new CNT walls. The samples treated longer than 30 min had much more disordered PyC deposited on the surface and the additional material did not form additional tube walls after thermal annealing.

1. Introduction

Carbon/carbon (C/C) composites are often produced by chemical vapor infiltration (CVI) of carbon source gases into fiber preforms. While CVI of carbon fiber structures has been the industrial standard, there is a growing interest in infiltrating CNT structures and characterizing the resulting morphology. CNT/carbon (CNT/C) composites are attractive as advanced, high-performance materials due to their potential combination of outstanding mechanical, thermal, and electrical properties, low density and coefficient of thermal expansion, and the ability to retain high performance in non-oxidizing atmospheres to temperatures of approximately 3000 °C [1–3]. Applications of C/C composites in the aerospace and defense industries include aircraft brakes [4], rocket nozzles, re-entry vehicles, nose cones [5–7], engine components, protection tubes and high temperature fasteners [1]. While the above applications are currently filled by traditional carbon fiber C/C composites, CNT/C composites may eventually provide superior properties.

CNTs have been applied in C/C composites as a secondary reinforcement material to obtain better properties [8–15].

---

* Corresponding author.
E-mail address: philip_bradford@ncsu.edu (P.D. Bradford).

http://dx.doi.org/10.1016/j.carbon.2014.07.049
0008-6223/© 2014 Elsevier Ltd. All rights reserved.

Newer studies, however, utilize CNTs as the main filler material using a combination of chemical vapor deposition (CVD) and CVI to prepare CNT/C composites. Fabrication of CNT/C composites via CVI has been accomplished using multiple routes. Gong et al. [16,17] fabricated aligned CNT/C composites by CVI of pyrolytic carbon (PyC) on an CNT preforms and studied the morphology and microstructure of deposited PyC along with thermal and electrical properties of the composite. A similar aligned CNT/C composite was fabricated in a simultaneous process by combining CVD and CVI processes in one step [18]. Other than aligned CNT structures, CNT/C composites have also been fabricated using isotropic pre-compressed blocks of multi-walled carbon nanotubes (MWCNTs) [19].

Despite the increasing number of studies focusing on the mechanisms and morphology of PyC deposition on CNTs, there is a lack of understanding in the graphitization mechanism of CNT/C composites fabricated through CVI of PyC into CNT structures. Work exploring the influence of CNTs on graphitization of the carbon matrix has been instead mainly limited to CNT/C fabrication through polymer infiltration and pyrolysis. Separate studies performed by Tzeng et al. [20] and Lanticse-Diaz et al. [21] showed that CNTs can induce stress graphitization in resin-derived carbon matrices such as glass like carbon, which is known to be a non-graphitizing carbon. This work focuses on the changes in the structure and morphology of PyC coatings deposited onto AMWCNT sheets when samples were structurally annealed at high temperature. An understanding of the relationship between PyC coating thickness and morphology after high temperature annealing will be significant for those wanting to produce highly graphitic CNT/C composites.

2. Experimental

2.1. *Synthesis of MWCNTs*

Vertically aligned CNT arrays were fabricated using a modified version of the chlorine mediated chemical vapor deposition route [22]. The modified procedure is detailed in previous work [23]. In short, the arrays were grown on a quartz substrate in a tube furnace at 760 °C with acetylene as the carbon precursor and $FeCl_2$ (anhydrous 99.5% VWR) as the catalyst. The process gases consisted of acetylene (600 sccm), argon (395 sccm) and chlorine (5 sccm). Growth pressure was maintained at 3 Torr. After 15 min of growth, the system was allowed to cool to room temperature while purging with argon. The resulting arrays were $\sim$2 mm tall containing MWCNTs with an average diameter $\sim 29 \pm 8$ nm. The as-grown arrays were easily drawn into AMWCNT sheets.

After cleaning the furnace tube, the as-grown arrays were reloaded inside the tube furnace and underwent a chlorine treatment at 760 °C for 15 min while the pressure of the system was maintained at 3 Torr. High temperature chlorine treatments are known to purify CNTs of iron catalyst impurity [24]. Iron quickly reacts with chlorine at high temperatures to produce $FeCl_2$ which then vaporizes and leaves the process tube. After the chlorine treatment, energy dispersive X-ray spectroscopy showed that the iron level decreased from 1.5 to 0.53 wt%. Any iron remaining after the chlorine treatment was thought to reside inside of the CNTs. For this study it was important to remove as much iron as possible to avoid possible secondary reactions, to ensure that it would not influence the final morphology of the heat treated carbon structures.

2.2. *AMWCNT/C composite fabrication*

The concept of dry, continuous drawing of CNTs for fabrication of yarns [25–28] and AMWCNT sheets [29–32] is now quite common. This technique was used to produce the AMWCNT/C structures in this work. To minimize potential variability that naturally comes from batch CNT growth, all of the samples utilized in this study were produced from arrays from a single growth run. Fig. 1 shows a schematic of the processing of the AMWCNT/C sheets. First, single layer AMWCNT sheets were wrapped around multiple graphite frames for further processing. Single layer AMWCNT sheets were used in the first set of experiments to ensure maximum carbon deposition uniformity. The single sheets had a thickness of approximately 20 μm with a very low density (0.002 g/cm^3). This significantly reduced the potential of PyC coating variation due to diffusion length of the carbon source gases. In the next step, the AMWCNT wrapped graphite frames were placed inside the tube furnace and PyC was deposited on them using CVI, with acetylene as carbon source. Samples were heated in vacuum and once the temperature reached 800 °C, acetylene was released into the system at a flow rate of 600 sccm while pressure was maintained at 30 Torr for the desired deposition time (0, 10, 20, 30, 40 or 80 min). These samples are referred to as pristine, 10_C, 20_C, 30_C, 40_C and 80_C, respectively.

A portion of the PyC coated AMWCNT sheet was removed from each sample for analysis. The remaining portions of the samples were further heat treated in a high temperature furnace (RED DEVIL vacuum furnace WEBB 124) at 2150 °C (maximum furnace temperature) for five hours in an argon atmosphere. The supplied argon had an initial purity of 99.999%. An in-line Concoa 580–1600 series oxygen/H_2O trap was also used to further reduce the concentration of oxidizing gases. This trap is capable of reducing the oxygen content in a gas stream to less than 15 ppb. The heat treated samples were labeled and referred to as pristine_G, 10_G, 20_G, 30_G, 40_G and 80_G after heat treatment. Fig. 2 shows the steps taken to make the AMWCNT/C sheets.

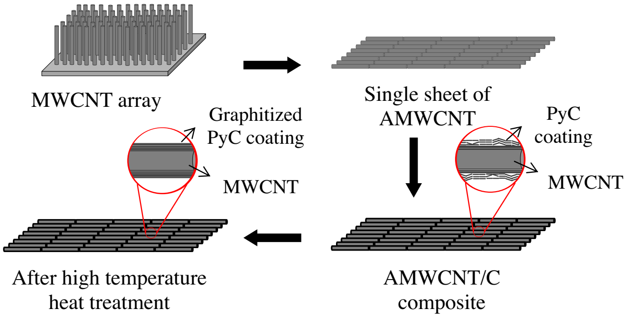

Fig. 1 – Schematic of a single sheet AMWCNT/C composite going through the multiple processing steps.

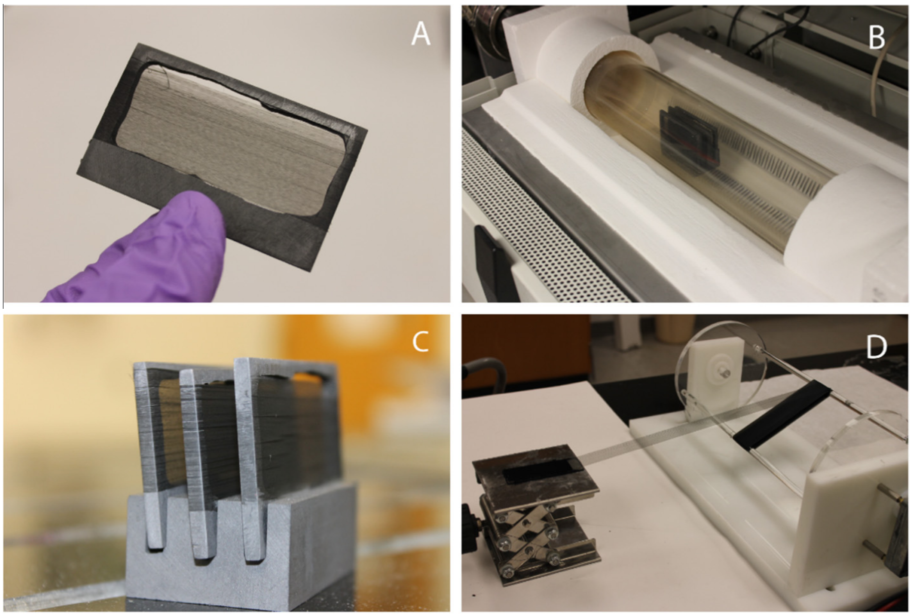

Fig. 2 – Procedure for AMWCNT/C composite sheet fabrication. (A) A single sheet of AMWCNT wrapped around a graphite frame. (B) AMWCNT wrapped graphite frames placed vertically onto a crucible holder inside the furnace for CVI of PyC. (C) Single sheets of AMWCNT/C after PyC deposition. (D) Dry drawing of thicker, multi-layer AMWCNT sheets.

These single sheet AMWCNT/C structures were used for Transmission Electron Microscopy (TEM) and Raman studies. Thicker samples were needed for X-ray diffraction (XRD), Thermogravimetric analysis (TGA) and electrical property analysis to increase accuracy of the measurements. To make thicker structures, the AMWCNT sheets were drawn from the array and continuously collected around two parallel glass rods rotating at 13 rpm. After 8 min of winding, the resulting multi-layer AMWCNT sheet was ~3 mm thick. These thick sheets were then separated from the glass rods using a razor and were placed inside the CVI furnace for PyC coating of 0, 30 or 80 min. This was followed by high temperature heat treatment of the samples. The conditions for PyC coating and heat treatment were the same as for the single layer AMWCNT/C sheets.

2.3. *Characterization*

Density values were calculated using the physical dimensions of the samples obtained by a calibrated scale bar in a stereo microscope, and the mass of the samples measured with an analytical balance with readability to 0.1 mg. After calculating the density of the pristine samples, they were PyC treated and the density was recalculated. The same samples were then heat treated and the density was recalculated again. Using the same samples throughout each step of the process allowed us to compare densities after each step without having a large number of samples.

TEM images were obtained using a JEOL 2000FX TEM operating at 200 kV. The TEM samples were prepared by dispersing a small amount of the AMWCNT/C sheet in chloroform using sonication. Following sonication, a droplet of the dispersion was deposited on a carbon mesh TEM grid and allowed to dry. To calculate the average diameter and diameter distribution, 100 measurements were taken from TEM images for each sample using ImageJ software. A Renishaw 2000 Raman microscope with a laser wavelength of 514 nm (50 × magnification) was used to analyze the quality of each structure. The single layer AMWCNT/C sheets were mounted to a microscope slide prior to spectrum acquisition and at least five spectra were obtained in different locations across each sample.

Diffraction experiments were performed on a PANalytical Empyrean diffractometer with a 7-circle goniometer configuration, using a Cu Kα source with a wavelength, $\lambda = 1.5406$ Å. A continuous, coupled scan ($2\theta - \varpi$) was taken for each sample for $2\theta = 20$–$60°$. As mentioned earlier, thicker samples were fabricated for X-ray, TGA and electrical property measurements. However, due to the low density of thick sheets and the interaction depth limitation, the signal strength for X-ray measurements was lower than expected. To increase signal intensity, samples were compressed and densified by infiltrating dilute epoxy solution and further curing the composite under pressure. A piece of quartz filter paper was placed under the composite before curing to absorb excess resin solution. The background for the amorphous epoxy and quartz was measured and subtracted from the final spectra for each sample. Samples were placed so that nanotubes were aligned parallel to the sample stage.

TGA experiments were conducted on a Perkin Elmer Pyris 1 TGA, where 5–10 mg of each sample was heated at a rate of 20 °C/min in air to 900 °C. Electrical properties of the AMWCNT/C sheets were measured using a four probe resistance measurement system. The samples were placed onto a glass plate across four parallel gold line electrodes. A square shaped piece of glass along with a 500 g weight was placed on top of the sample to ensure consistent contact between sample and all four gold electrodes during resistance measurements.

3. Results and discussion

Raman spectroscopy was used to compare the structure of arrays before and after the chlorine treatment. Generally, the G peak (centered around 1580 cm^{-1} in SWNT) originates from the perfect graphite crystal structure while D peak (centered around 1350 cm^{-1} in SWNT) originates from the defects in the structure [33]. The integrated intensity ratio of disordered to graphitic carbon ($R = I_D/I_G$) was used to evaluate the defect density of carbon materials [34]. After the chlorine treatment, the average R changed from 0.45 to 0.41 indicating a slight improvement in the quality of the MWCNT arrays. Raman spectra of the arrays collected before and after chlorine treatment are provided in the Supporting information.

Table 1 shows the variation in average CNT diameter with PyC deposition time. CNT diameter increased significantly with increasing CVI time. The thickness of the PyC layer (half of the difference between diameter of PyC coated CNTs and pristine CNT diameter) increased from 3 nm after 10 min PyC deposition to 34 nm after 80 min PyC deposition. The diameter distribution of coated CNTs also broadened as deposition time increased. The use of a single layer CNT sheet ruled out the possibility of deposition variation due to a diffusion length limitation. The reason for a larger diameter distribution for longer PyC coating times is not understood at this time.

Fig. 3 shows density variation with different PyC coating times, before and after high temperature heat treatment. Pristine sheets of AMWCNTs (0 min carbon treatment time) are very low density structures with apparent density of ~0.002 g/cm^3. After 30 and 80 min of PyC deposition, apparent density increased to 0.004 and 0.007 g/cm^3 respectively. Density of the structures did not change significantly after high temperature heat treatment. The outer dimensions of the multi-layer AMWCNT sheet samples did not change after PyC deposition or heat treatment. While the mass (and therefore density) of the PyC coated structures increased fairly linearly with coating time, the change in tube diameter did not. The much larger tube diameters at the longest deposition time were attributed to the decreasing level of structural order and corresponding decreased local density of the outermost PyC layers.

Table 1 – Average CNT diameter for different PyC deposition times.

Infiltration time (min)	Avg CNT diameter (nm)
0	29 ± 8
10	35 ± 7
20	37 ± 7
30	44 ± 10
40	50 ± 12
80	97 ± 16

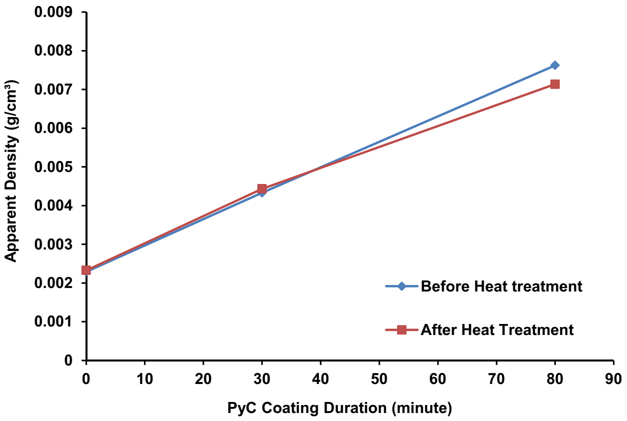

Fig. 3 – Changes in the density of thick multi-layered AMWCNT/C sheets with different PyC coating durations.

While the CNT diameters were increased significantly, it is unlikely that this increase (and subsequent narrowing of the space between the CNTs) had an effect on the deposition mechanism of the PyC as the deposition time increased. Even the AMWCNT/C sheet samples treated for the longest time of 80 min had an aerogel-like density, with CNT packing density lower than even the as-grown CNT array. This highly porous nature, where inter-tube spacing is hundreds of nanometers [23], is conducive for gas diffusion through the structure at the deposition pressure utilized in this study.

3.1. *Morphology of AMWCNT/C composites*

TEM images in Figs. 4 and 5 show the structures of samples coated for 10, 20, 30, 40 and 80 min before and after heat treatment. Generally, the deposited PyC exhibited two morphologies, transitioning from rough laminar PyC deposited on the surface of CNTs toward disordered carbon at the outermost surface of the coating. While this is consistent with previous reports [19,35], it is different from results reported by Allouche et al. [36–38], where little to no difference in the quality of PyC coating was observed in layers close to the surface of fibers compared to those near the center. Further comparison between these images in Figs. 4 and 5 show that by increasing carbon treatment time and thickening the PyC layer, the deposited layers became more disordered and contained more curved carbon segments which resulted in disinclination of parallel carbon layers and thus, the surface of the coating layer became less smooth and less dense. One of the possible reasons for this is further explored in Section 3.3.

The PyC layer was also discontinuous in some areas across the length of CNTs. Zheng et al. observed this as well and proposed that this variation occurred because “some layers stopped growing laterally due to the edges of graphenes were blocked by the top layer” [35]. Another possible reason is that at some points, the MWCNTs within the sheet were touching each other which would suppress PyC deposition in those areas. Those CNTs would then become separated after dispersion.

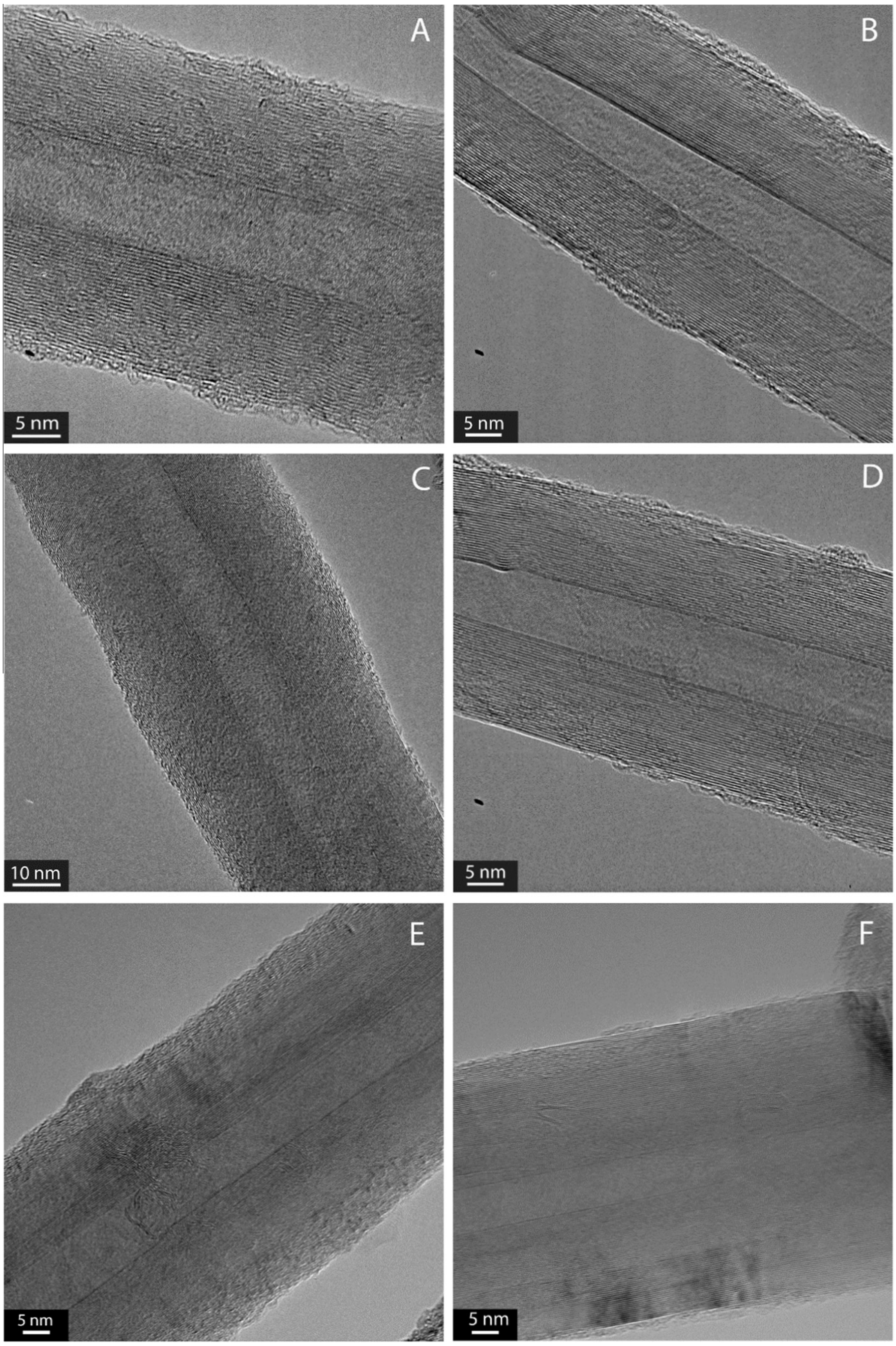

Fig. 4 – TEM images of PyC coated CNTs before (left column) and after (right column) heat treatment for samples with 10 min (A and B), 20 min (C and D) and 30 min (E and F) PyC coating.

Images of samples exposed to the heat treatment at 2150 °C for five hours showed fewer structural defects in the walls and improved graphitic quality of both the CNT structure and the deposited PyC coating layer. For samples with shorter carbon deposition times (10_G, 20_G and 30_G), the PyC layer rearranged, resulting in a crystalline structure where the coating and original tube walls could not be easily differentiated in the TEM images. In contrast, images of 40_G and 80_G samples showed that while the PyC layers deposited closest to the original MWCNT developed a structure similar to the CNT walls, carbon layers close to the surface exhibited a more disordered PyC structure, and remained disordered even after the heat treatment.

3.2. *Structure of AMWCNT/C sheets*

Raman spectroscopy was used to analyze the graphitic structure of pristine and AMWCNT/C sheets. Of particular interest were the G peak and D peak, as they contribute to graphitic and disordered carbon structures respectively. Each sample was scanned at 5 different locations and the average R (I_D/I_G) was calculated. As shown in Fig. 6, increasing the PyC

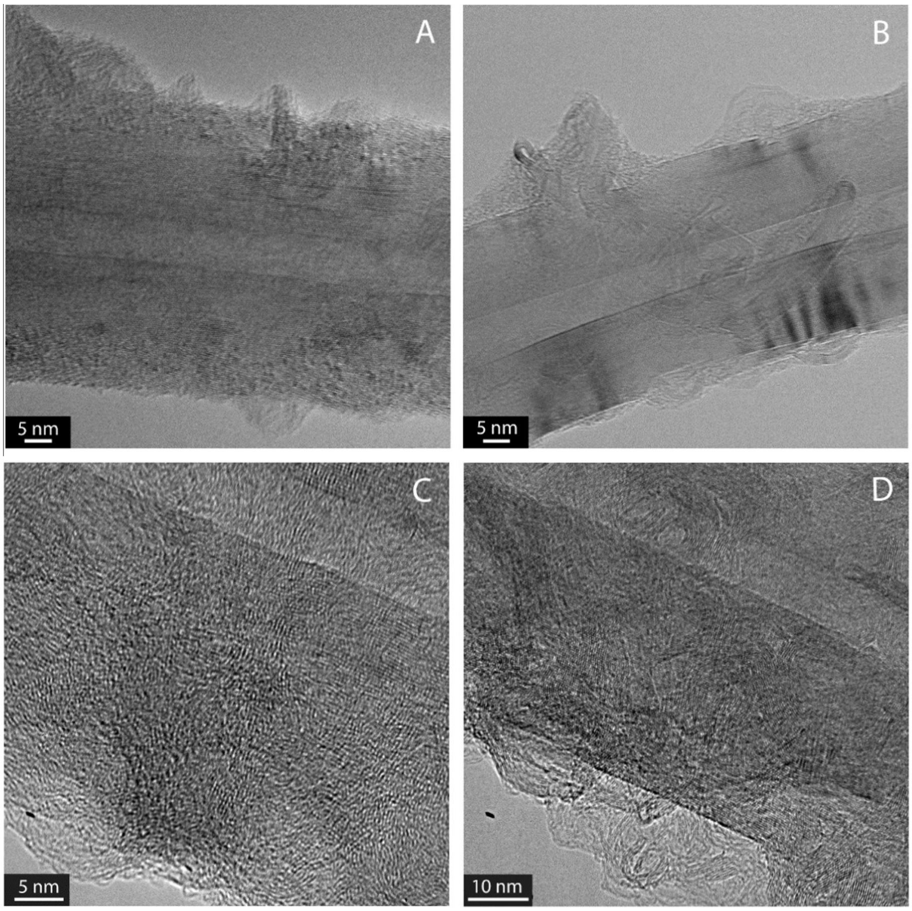

Fig. 5 – TEM images of PyC coated CNTs before (left column) and after (right column) heat treatment for samples with 40 min (A and B) and 80 min (C and D) PyC coating.

infiltration time increased the average value of R from 0.36 for pristine AMWCNT sheet to 2.12 after 80 min PyC infiltration. This indicates that thickening the AMWCNTs with PyC increases the structural disorder. After heat treatment at 2150 °C, the average R for AMWCNT sheets with 10, 20 and 30 min PyC deposition all decreased to ~0.2. This average R ratio was very close to that of the pristine AMWCNT sheet after the same high temperature heat treatment (~0.17). While the average R ratios of samples with longer PyC infiltration times (≧40 min) also decreased after heat treatment, they yielded higher ratios compared to PyC coated samples treated for shorter times. In addition to the decrease in R ratio, a smaller full width half maximum of both the G band and D band was observed after high temperature heat treatment of the samples. The decreased scattering after annealing indicates a high level of CNT structural uniformity and has been reported in previous studies of annealed CNTs [39,40]. Raman spectra of pristine and PyC coated AMWCNT sheets before and after annealing are provided in the Supporting information. The Raman results support the results from TEM observations and show that there is a limit for the thickness of PyC coating that allows for radial growth of graphitic CNT walls after high temperature heat treatment. For the deposition parameters used in this study, this limit was approximately 30 min, after which the additional deposited layer did not reorganize to resemble tube walls and radially grow the MWCNT structure. It is important to note that with different deposition conditions, precursors or original CNT characteristics, the structure of the deposited PyC will be different [41] and thus the maximum thickness of PyC that can structurally annealed into new tube walls may be different as well.

XRD spectra of pristine, AMWCNT/C, and heat treated samples are shown in Fig. 7. Due to the parallel z-axis orientation of the CNTs to the incident beam, the main visible features are the 001 reflections at 002 (~26°). Based on the position of the 002 peak, information about the average interlayer spacing, or d-spacing, can be calculated using the Bragg equation, $d_{002} = \lambda/2\sin\theta_{002}$. Additionally, the full width half maximum (FWHM) of this peak can be used to calculate the graphite stack size or crystallite size (L_c), using Scherrer's equation, $L_c = \lambda/\beta\cos\theta_{002}$ [42]. In these equations, λ is the X-ray wavelength, θ_{002} is the location of the 002 reflection, and β is the FWHM of the 002 peak. The measured and calculated parameters for each sample are summarized in Table 2.

PyC deposited samples have larger d-spacings than pristine CNTs. This indicates that the as-deposited material was rough and poorly graphitized, which is confirmed in the TEM images. The measurable increase in intensity of the 002 peak after heat treatment indicates improvement in the interlayer graphitic structure due to removal of defects and carbon atom rearrangement. Significant changes were measured in the stack size of graphite crystallites. L_c for pristine

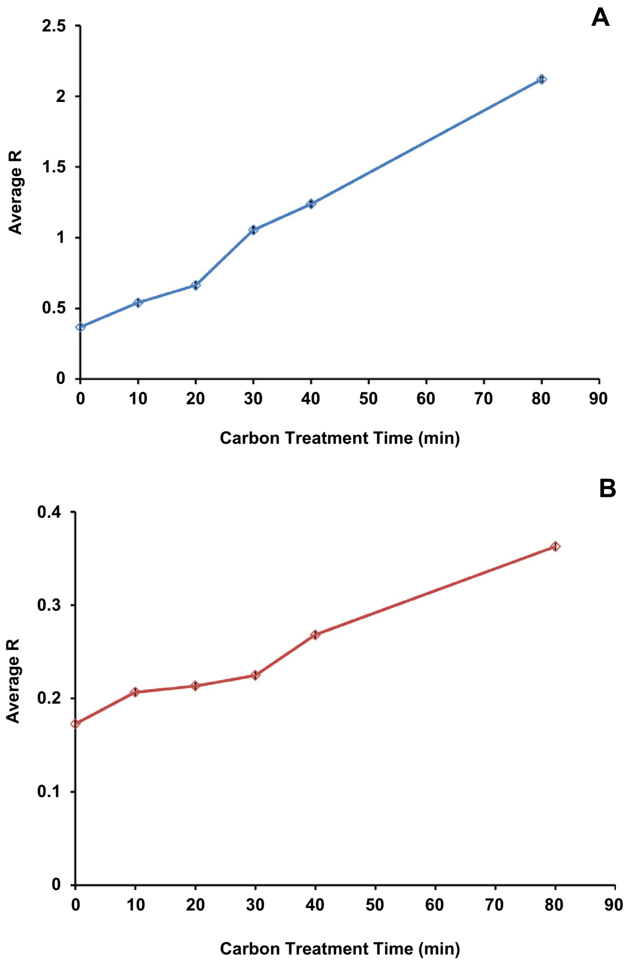

Fig. 6 – Average R as a function of PyC coating duration before (A) and after heat treatment (B).

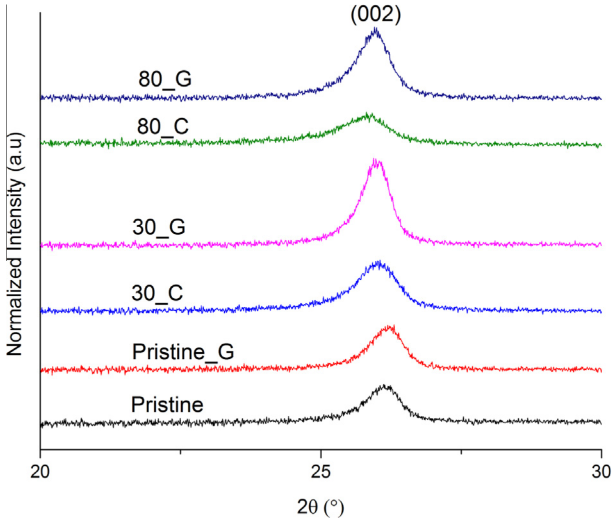

Fig. 7 – XRD spectra of pristine, PyC coated and heat treated samples.

was 13.29 nm, and by dividing this number by the characteristic d-spacing, the number of walls, *n*, was found to be 39. L_c increased after annealing sample 30_C due to the radial growth of CNTs and the formation of additional walls, leading to an increase in n from 39 to 45. L_c did not continue to increase for sample 80_G however, due to the inability to fully graphitize the deposited PyC during structural annealing. These findings are in agreement with TEM images and Raman results. The decrease in L_c and *n* for 30_C and 80_C and G arises from the disordered structure so that the XRD parameters cannot fully represent the structure of those samples [19].

Fig. 8 shows the TGA and derivative TGA curves of the samples. Small mass loss was observed to occur between 200 and 400 °C which was due to the presence of amorphous carbon. The relatively minute amount of mass loss that occurred in this region for all samples (even those deposited with PyC carbon) indicates that they were relatively free of bulk amorphous carbon. The small loss could be attributed to broken or incomplete surface layers of carbon, which would be highly reactive with the oxygen in air. The average onset temperature for AMWCNT sheets prior to heat treatment was 625 °C. After high temperature heat treatment of the samples, the average onset temperature was increased to nearly 750 °C. Annealing healed some of the defects in MWCNTs and PyC coatings, leaving a structure with greater oxidative stability [43].

To support findings from TEM, Raman and XRD analysis, the electrical conductivity of the AMWCNT/C sheets were measured before and after high temperature heat treatment. As shown in Table 3, conductivity of pristine AMWCNT sheets increased from 2.03 to 4.1 S/cm after 80 min PyC treatment with subsequent annealing. This increase was reasonable due to the addition of electrically conductive material on the original CNT structure of the same physical dimensions. Some of PyC would be deposited at CNT junctions, reducing the contact resistance between CNTs [19]. High temperature heat treatment also improved the conductivity of all of the samples. The results show that the largest increase in conductivity before and after heat treatment was 60%, for the composite with 30 mins PyC deposition. This supports Raman and XRD data, corresponding well to the structural changes identified in that sample. The 30-G sample had the largest tube diameter and mass increases while still being graphitized well during the high temperature heat treatment. Further PyC deposition increased the mass and diameter of the CNTs, however the inability for the additional layers to graphitize limited the increase in electrical conductivity after heat treatment to 37%.

3.3. *Effect of MWCNTs quality on the microstructure of PyC coating*

Results from TEM observations suggest that the ordered structure of carbon atoms in the initial PyC coating layers was induced by CNTs. Gong et al. [16,44] reported formation of a highly-textured, rough laminar PyC coating on CNTs, while a smooth laminar structure was formed on carbon fibers. Here, to further study the effect of graphitic quality of CNTs on the microstructure of deposited PyC, a single layer sheet of pristine AMWCNT was first annealed at 2150 °C for five hours and then coated with PyC for 40 mins. Fig. 9 shows a TEM image of this sample (labeled G-40-C). A comparison between this image and Fig. 5a (for sample 40-C) shows that

Table 2 – Measured and calculated structural parameters of the different samples.

Sample	2θ (degree)	d_{002} (Å)	FWHM (degree)	L_c (nm)	n
Pristine	26.1	3.412	0.7398	13.29	38.95
Pristine_G	26.16	3.403	0.7194	13.67	40.16
30_C	25.99	3.426	0.8855	11.09	32.37
30_G	25.97	3.428	0.6284	15.63	45.58
80_C	25.75	3.458	1.109	8.836	25.55
80_G	25.92	3.434	0.8333	11.78	34.30

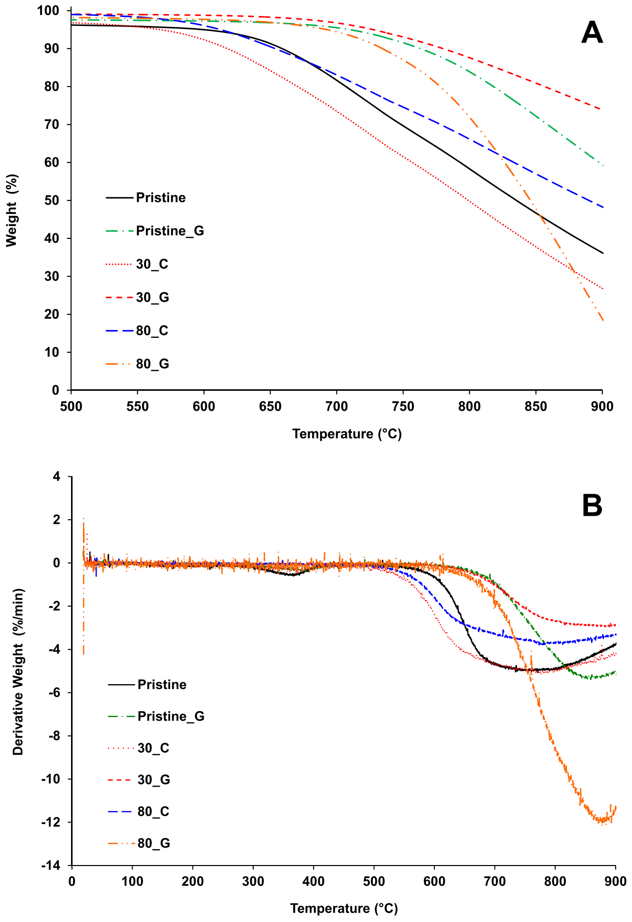

Fig. 8 – TGA curves (A) and derivative TGA curves (B) of pristine and PyC coated samples.

Table 3 – Electrical conductivity of AMWCNT sheets with different PyC coating times.

Sample	Conductivity (S/cm)	Percent increase (%)
Pristine	2.03	32
Pristine_G	2.67	
30_C	2.47	60
30_G	3.98	
80_C	2.98	37
80_G	4.10	

despite having the same infiltration time of 40 min, the PyC coating in G_40_C is more ordered and the outermost surface is smoother. The CNTs with higher quality graphitic walls induced the ordered structure in PyC coating layer over a longer range, which may allow for a further increase in the thickness of PyC that can be recrystallized on the surface of the CNTs. These results also help to explain why the PyC coating on the as-grown CNTs transitions from a rough laminar carbon to disordered carbon as the coating thickness increases. It appears that the quality of the PyC deposited during this process depends of the surface quality of the underlying tube structure (pristine tube or one that has PyC deposited on it). Future work may include a more detailed study in this area.

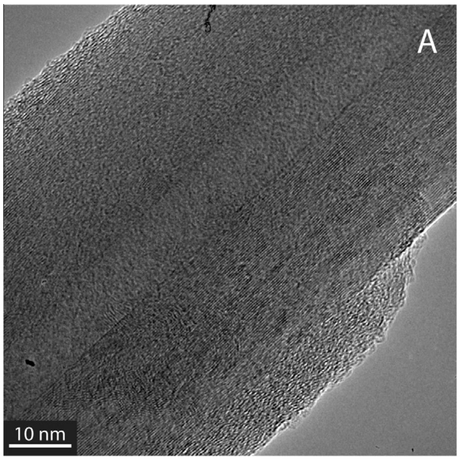

Fig. 9 – TEM images of 40 min PyC coating on a graphitized pristine CNT.

4. Conclusions

Aligned multi-walled carbon nanotube/Carbon sheets were prepared using AMWCNT sheets and CVI of PyC for different time periods. Results showed that while annealing PyC coated samples at 2150 °C for five hours will radially grow additional walls on nanotubes, there is a limit to the thickness of PyC coating layer that can be annealed into additional MWCNT walls. Raman studies revealed that annealing MWCNT sheets with shorter PyC coating times (up to 30 mins) graphitized the coating layer to a large extent. Further thickening of the PyC layer by increasing carbon infiltration time (to 40 and 80 mins) did not yield a coating that resembled nanotube walls after annealing. These results agreed with XRD findings which showed that the average number of tube walls increased from 39, for pristine nanotubes, to 45 for samples coated with PyC for 30 mins and then annealed (30_G). The number of graphitic walls did not continue to increase, however, for samples with longer carbon treatment times. TEM images and electrical property measurements also supported the above findings.

Acknowledgements

This work was supported by the Air Force Office of Scientific Research project number FA9550-12-1-0088. The authors acknowledge the use of the Analytical Instrumentation Facility (AIF) at North Carolina State University, which is supported by the State of North Carolina and the National Science Foundation.

Appendix A. Supplementary data

Supplementary data associated with this article can be found, in the online version, at http://dx.doi.org/10.1016/j.carbon.2014.07.049.

REFERENCES

[1] Manocha LM. High performance carbon–carbon composites. Sadhana 2003;28(1–2):349–58.
[2] Luo R, Zhang J, Li J, Zhang Y, Zhang J, Su C. Carbon/carbon composites. Wiley Encyclopedia of Composites; 2012.
[3] Fitzer E. The future of carbon–carbon composites. Carbon 1987;25(2):163–90.
[4] Hutton TJ, McEnaney B, Crelling JC. Structural studies of wear debris from carbon–carbon composite aircraft brakes. Carbon 1999;37(6):907–16.
[5] Sheehan JE, Buesking KW, Sullivan BJ. Carbon–carbon composites. Annu Rev Mater Sci 1994;24:19–44.
[6] Windhorst T, Blount G. Carbon–carbon composites: a summary of recent developments and applications. Mater Des 1997;18(1):11–5.
[7] Krenkel W, Berndt F. C/C–SiC composites for space applications and advanced friction systems. Mater Sci Eng:A 2005;412(1–2):177–81.
[8] Chen J, Xiong X, Xiao P. The effect of carbon nanotube growing on carbon fibers on the microstructure of the pyrolytic carbon and the thermal conductivity of carbon/carbon composites. Mater Chem Phys 2009;116(1):57–61.
[9] Gong Q, Li Z, Zhou X, Wu J, Wang Y, Liang J. Synthesis and characterization of in situ grown carbon nanofiber/nanotube reinforced carbon/carbon composites. Carbon 2005;43(11):2426–9.
[10] Gong Q, Li Z, Zhang Z, Wu B, Zhou X, Huang Q, et al. Tribological properties of carbon nanotube-doped carbon/carbon composites. Tribol Int 2006;39(9):937–44.
[11] Lim D, An J, Lee HJ. Effect of carbon nanotube addition on the tribological behavior of carbon/carbon composites. Wear 2002;252:512–7.
[12] Li X, Li K, Li H, Wei J, Wang C. Microstructures and mechanical properties of carbon/carbon composites reinforced with carbon nanofibers/nanotubes produced in situ. Carbon 2007;45:1662–8.
[13] Song Q, Li K, Li H, Li H, Ren C. Grafting straight carbon nanotubes radially onto carbon fibers and their effect on the mechanical properties of carbon/carbon composites. Carbon 2012;50(10):3949–52.
[14] Xiao P, Lu X, Liu Y, He L. Effect of in situ grown carbon nanotubes on the structure and mechanical properties of unidirectional carbon/carbon composites. Mater Sci Eng:A 2011;528(7–8):3056–61.
[15] Li K, Li L, Li H, Song Q, Lu J, Fu Q. Electrophoretic deposition of carbon nanotubes onto carbon-fiber felt for production of carbon/carbon composites with improved mechanical and thermal properties. Vacuum 2014;104:105–10.
[16] Gong Q, Li Z, Li D, Bai X, Liang J. Fabrication and structure: a study of aligned carbon nanotube/carbon nanocomposites. Solid State Commun 2004;131(6):399–404.
[17] Gong Q, Li Z, Bai X, Li D, Zhao Y, Liang J. Thermal properties of aligned carbon nanotube/carbon nanocomposites. Mater Sci Eng:A 2004;384(1–2):209–14.
[18] Li X, Ci L, Kar S, Soldano C, Kilpatrick SJ, Ajayan PM. Densified aligned carbon nanotube films via vapor phase infiltration of carbon. Carbon 2007;45(4):847–51.
[19] Jin Y, Zhang Y, Zhang Q, Zhang R, Li P, Qian W, et al. Multiwall carbon nanotube-based carbon/carbon composites with three-dimensional network structures. Nanoscale 2013;5(13):6181–6.
[20] Tzeng S, Lin Y. Formation of graphitic rods in carbon/carbon composites reinforced with carbon nanotubes. Carbon 2013;52:617–20.
[21] Lanticse-Diaz LJ, Tanabe Y, Enami T, Nakamura K, Endo M, Yasuda E. The effect of nanotube alignment on stress graphitization of carbon/carbon nanotube composites. Carbon 2009;47(4):974–80.
[22] Inoue Y, Kakihata K, Hirono Y, Horie T, Ishida A, Mimura H. One-step grown aligned bulk carbon nanotubes by chloride mediated chemical vapor deposition. Appl Phys Lett 2008;92(21). 213113-213113-3.
[23] Yildiz O, Bradford PD. Aligned carbon nanotube sheet high efficiency particulate air filters. Carbon 2013;64:295–304.
[24] Chng ELK, Poh HL, Sofer Z, Pumera M. Purification of carbon nanotubes by high temperature chlorine gas treatment. Phys Chem Chem Phys 2013;15:5615–9.
[25] Zhu HW, Xu CL, Wu DH, Wei BQ, Vajtai R, Ajayan PM. Direct synthesis of long single-walled carbon nanotube strands. Science 2002;296:884–6.
[26] Jiang K, Li Q, Fan S. Nanotechnology: spinning continuous carbon nanotube yarns. Nature 2002;419:801.
[27] Zhang X, Li Q, Holesinger TG, Arendt PN, Huang J, Kirven PD, et al. Ultrastrong, stiff, and lightweight carbon-nanotube fibers. Adv Mater 2007;19(23):4198–201.
[28] Thiagarajan V, Wang X, Bradford P, Zhu YT, Yuan FG. Stabilizing carbon nanotube yarns using chemical vapor infiltration. Composites Sci Technol 2014;90:82–7.
[29] Inoue Y, Suzuki Y, Minami Y, Muramatsu J, Shimamura Y, Suzuki K, et al. Anisotropic carbon nanotube papers fabricated from multiwalled carbon nanotube webs. Carbon 2011;49(7):2437–43.
[30] Liu W, Zhang X, Xu G, Bradford PD, Wang X, Zhao H, et al. Producing superior composites by winding carbon nanotubes onto a mandrel under a poly(vinyl alcohol) spray. Carbon 2011;49(14):4786–91.
[31] Wang X, Yong ZZ, Li QW, Bradford PD, Liu W, Tucker DS, et al. Ultrastrong, stiff and multifunctional carbon nanotube composites. Mater Res Lett 2013;1(1):19–25.
[32] Zhou Z, Wang X, Faraji S, Bradford PD, Li Q, Zhu Y. Mechanical and electrical properties of aligned carbon nanotube/carbon matrix composites. Carbon 2014;75:307–13.
[33] Dresselhaus MS, Dresselhaus G, Saito R, Jorio A. Raman spectroscopy of carbon nanotubes. Phys Rep 2005;409(2):47–99.
[34] Cancado L, Takai K, Enoki T, Endo M, Kim Y, Mizusaki H, et al. General equation for the determination of the crystallite size L a of nanographite by Raman spectroscopy. Appl Phys Lett 2006;88. 163106,163106-3.

[35] Zheng G, Sano H, Uchiyama Y. A layer-by-layer deposition mechanism for producing a pyrolytic carbon coating on carbon nanotubes. Carbon 2013;57:267–73.

[36] Allouche H, Monthioux M, Jacobsen RL. Chemical vapor deposition of pyrolytic carbon on carbon nanotubes: Part 1: synthesis and morphology. Carbon 2003;41(15):2897–912.

[37] Allouche H, Monthioux M. Chemical vapor deposition of pyrolytic carbon on carbon nanotubes: Part 2: texture and structure. Carbon 2005;43(6):1265–78.

[38] Monthioux M, Allouche H, Jacobsen RL. Chemical vapour deposition of pyrolytic carbon on carbon nanotubes: Part 3: growth mechanisms. Carbon 2006;44(15):3183–94.

[39] Behler K, Osswald S, Ye H, Dimovski S, Gogotsi Y. Effect of thermal treatment on the structure of multi-walled carbon nanotubes. J Nanopart Res 2006;8:615–25.

[40] Gong Q, Li Z, Wang Y, Wu B, Zhang Z, Liang J. The effect of high-temperature annealing on the structure and electrical properties of well-aligned carbon nanotubes. Mater Res Bull 2007;42(3):474–81.

[41] Delhaes P. Chemical vapor deposition and infiltration processes of carbon materials. Carbon 2002;40:641–57.

[42] Vix-Guterl C, Couzi M, Dentzer J, Trinquecoste M, Delhaes P. Surface characterizations of carbon multiwall nanotubes: comparison between surface active sites and Raman spectroscopy. J Phys Chem B 2004;108(5):19361–7.

[43] Bom D, Andrews R, Jacques D, Anthony J, Chen B, Meier MS, et al. Thermogravimetric analysis of the oxidation of multiwalled carbon nanotubes: evidence for the role of defect sites in carbon nanotube chemistry. Nano Lett 2002;2(6):615–9.

[44] Gong Q, Li Z, Bai X, Li D, Liang J. The effect of carbon nanotubes on the microstructure and morphology of pyrolytic carbon matrices of C–C composites obtained by CVI. Composites Sci Technol 2005;65(7–8):1112–9.